Vol. **114** (2008) *ACTA PHYSICA POLONICA A* Supplement

Proceedings of the Professor Stefan Mróz Symposium

Dependence of STM Images on Bias Polarity for Sm Layers on Mo(110) and Mo(211) Surfaces

M. Kuchowicz*, R. Szukiewicz and D. Grodzińska

Institute of Experimental Physics, University of Wrocław
pl. M. Borna 9, 50-204 Wrocław, Poland

Thin Sm layers adsorbed on Mo(110) and (211) surfaces were studied with scanning tunneling microscope. It was found that obtained images of these adsorption systems significantly depend on the polarity of the scanning tunneling microscope bias voltage. This dependence is more pronounced for the Sm on Mo(110) than on Mo(211). For Sm/Mo(110), at low Sm coverages the change of bias polarity results in significant difference in the measured height of the adsorbed Sm layer, while the heights of substrate terraces remain the same for both signs of the applied bias voltage. In the coverage range $0.65 < \theta < 1$, scanning tunneling microscope images, obtained with negative bias, show the gaps in Sm layers, which are invisible for positive bias.

PACS numbers: 68.37.Ef, 68.37.–d, 71.20.Eh

1. Introduction

The scanning tunneling microscope (STM) has been a very powerful tool for investigations of structures of surfaces of metals and semiconductors as well as of thin adsorbed layers [1–4]. However, STM images stem from both atomic and electronic structures of surfaces [3, 5], which complicates interpretation of the obtained results. Thus, it is well established that surface atoms in metallic systems are usually imaged as protrusions for both positive and negative bias voltages. In contrast, oxygen atoms adsorbed on transition metal surfaces can be seen as depressions or protrusions depending on the polarity and magnitude of the bias [6–9]. In nanometer scale, STM images, obtained with different signs of bias voltages for metallic systems, again, are usually very similar, while semiconductor surfaces demonstrate a strong dependence of STM images on the bias sign.

This effect is caused by different tunneling conditions for electrons going from the tip to the surface (when the tip bias is negative) and electrons going from the surface to the tip (when the bias is positive). Accordingly, different electronic

*corresponding author; e-mail: macko20@ifd.uni.wroc.pl

states give rise to the STM current, namely, states within the energy range from E_F to $E_F + eV$ or from E_F to $E_F - eV$, so that the current depends on the local density of states (LDOS) at the surface in these energy ranges. In simple metals the dependence of LDOS on energy is rather smooth, and the switch of bias does not affect STM images significantly. For semiconductor surfaces this electronic effect can be very pronounced, sometimes leading to quite different images and estimated heights of surface steps [3].

For surfaces of rare earth metals, which are particularly interesting due to unusual electronic properties arising from highly localized $4f$ electrons [10], it can be expected that obtained STM images will depend on the sign of bias because of possible presence of occupied or empty f bands in vicinity of E_F. Gd thin layers were widely investigated with STM and scanning tunneling spectroscopy (STS) techniques [11–15]. It was found that Gd islands on W(110) were imaged differently for different tunneling conditions. In particular, flat areas of islands, visible in STM images obtained with negative bias, for positive bias were "subsided" with pronounced decoration around them [14]. A strong dependence of the height of apparent surface steps observed with STM on the sign of bias was recently reported for Gd layers on Mo(112) [11]. The apparent surface corrugation was found for the bias voltage corresponding to the tunneling involving the occupied bulk bands and explained in terms of band symmetry for observed Gd structures.

In this regard, samarium metal presents a very interesting case due to a narrow f-derived peak in LDOS near below E_F [16], and therefore new effects in the dependence of STM images on the bias voltage can be expected. It is generally believed that Sm has two different valence states, namely, trivalent ([Xe] $4f^5$ $(5d6s)^3$ — Sm^{3+}) in the bulk metal while divalent ([Xe] $4f^6$ $(5d6s)^2$ — Sm^{2+}) at surface. Moreover, the diameter of Sm^{3+} atom is 3.61 Å [10], while of Sm^{2+} is 4.04 Å [10, 17]. The issue of Sm valence has been studied in a great number of papers devoted to investigations of the Sm thin films deposited on various metallic [18–25] and semiconductor substrates [26–29]. However, STM investigations of Sm surfaces are scarce, and we are aware of only a few papers concerning STM investigations for Sm layers on Si(111) and Si(100) [27, 28], on Mo(110) [20], and on low-index Cu surfaces [24, 25].

It should be mentioned that recent theoretical calculations [16] have shown that both [Xe] $4f^5$ $(5d6s)^3$ and [Xe] $4f^6$ $(5d6s)^2$ starting configurations of Sm, due to self-consistent redistribution of valence electrons, result in the same local density of states. The calculated LDOS resembles only those peaks in photoemission spectra, which are believed to be pertinent to divalent Sm (that is, located about –2 eV with regard to E_F), while observed peaked structure about –5 eV has been attributed not to Sm^{3+}, but to the influence of surface contaminations like O or H [16].

The hydrogenation of rare earth metals leads to a significant (22% for GdH_3) volume expansion [30–33]. The rare-earth metals hydrides are isolators or semi-

conductors provided that the number of H atoms per one rare-earth atom is more than 2 [30, 34]. As such, the decorations of steps and dependence on the bias for STM images of hydrogenated thin Gd layers on W(110) [35] may be attributed to known effects pertinent to semiconductor surfaces. Similar consideration seems reasonable also for Sm. To our best knowledge, no microscopic investigations of hydrogen-exposed Sm layers have been reported to date.

2. Experiment

The STM (Omicron) ultra-high (better than 1×10^{-10} Torr) vacuum chamber was equipped with a spherical retarding field analyzer (RFA), used for low energy electron diffraction (LEED) and Auger electron spectroscopy (AES), and a quadrupole mass spectrometer (QMS) for thermal desorption spectroscopy (TDS). The deposition of Sm was performed at room temperature. In the preparation chamber, the sample could be heated up to 2000 K.

The Mo(110) and Mo(211) samples were cut off from a single Mo monocrystal (of 5N purity). The surfaces were parallel to (110) and (211) crystal planes with accuracy of $\pm 0.05^\circ$. The samples were cleaned using a standard procedure, which included extensive heating at 1200–1300 K in oxygen atmosphere at 10^{-7} Torr, followed by several high-temperature flashes at 2300–2400 K. The samples were believed to be free from impurities when the Auger amplitude (AA) of carbon (272 eV) was at least 300 times lower than that of molybdenum (186 eV).

Metallic Sm (of 3N purity) was used for deposition. The Sm was evaporated from a molybdenum crucible, heated by a tungsten heating coil warped around it. Empty crucible was positioned into an auxiliary vacuum apparatus, where the heating to 2000 K was performed for several hours. Then the crucible with a piece of Sm metal was transferred (in Ar gas atmosphere) and mounted again in the auxiliary vacuum apparatus for outgasing. After several days of outgasing, the Sm source was transferred (again, in Ar gas atmosphere) to the STM chamber.

The STM head was calibrated by using the (7×7) reconstructed Si(111) surface as well as the Mo(211) surface [36]. STM measurements were performed in the constant tunneling current mode. The sample during measurements was grounded, so the bias voltage was applied to the tip. The STM images were processed using the WSxM software from Nanotec Electronica [37].

3. Results and discussion

STM images, obtained for Sm coverage $\theta \approx 0.1$ ML on Mo(110), are shown in Fig. 1. For a negative bias (Fig. 1a), the measured height of Sm islands is of 1.8 ± 0.1 Å, while for a positive bias (Fig. 1b) it diminishes to 0.5 ± 0.1 Å. In contrast, the height of Mo(110) terraces remains unchanged on switching the polarity of the bias and corresponds to the Mo{110} interplane distance in a bulk crystal (2.23 Å).

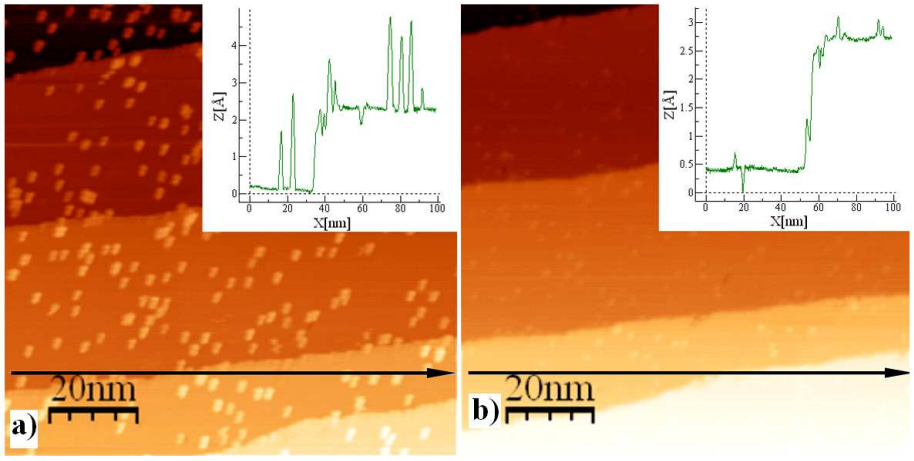

Fig. 1. STM images of 0.1 ML Sm/Mo(110) at negative and positive biases. 100×100 nm^2, $U = -2$ V, $I_t = 0.5$ nA (a); 100×100 nm^2, $U = 2$ V, $I_t = 0.5$ nA (b).

Already at $\theta = 0.3$ ML, LEED reveals the formation of the c(7×2) structure, and STM images, obtained with a positive bias (Fig. 2a), show that almost the whole surface is covered by a smooth adsorbate layer. In contrast, STM images, obtained with a negative bias (Fig. 2b), reveal some areas with different atom arrangements.

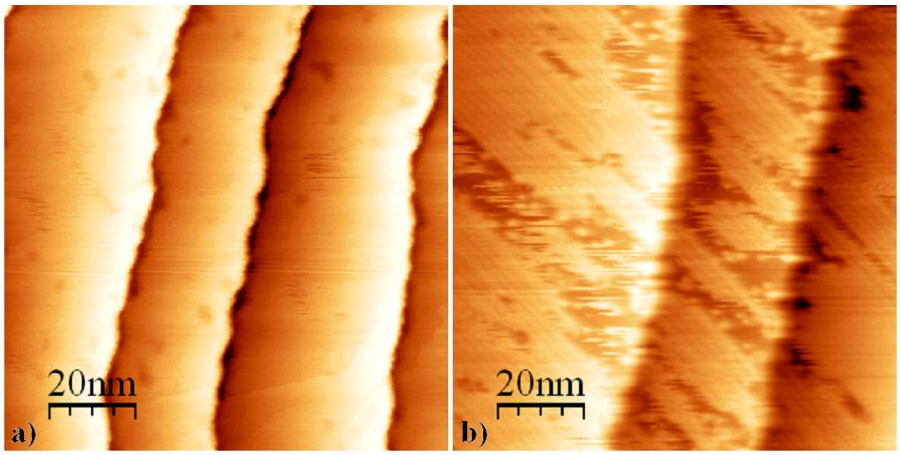

Fig. 2. STM images of 0.4 ML Sm/Mo(110) at positive and negative biases. 100×100 nm^2, $U = 2$ V, $I_t = 1$ nA (a); 100×100 nm^2, $U = -2$ V, $I_t = 1$ nA (b).

During STS experiments (at vacuum 5×10^{-10} Tr) we observed Sm islands. After obtaining STM images, presented in Fig. 3, we attempted STS measurements, but the island suddenly exploded. The next scan revealed that a large

surface area became covered by small Sm agglomerates with no trace of the island (Fig. 3c) seen before. Taking into account that rare-earth metals (RE) compounds with hydrogen (REH_x where $2 < x < 3$) have lattice constant greater over 20% than in case of pure metals [30–33], electric field created by tip could lead to change of H atoms per rare-earth atom and stress rises inside island. This stress could be responsible for destroying islands during STS measurements.

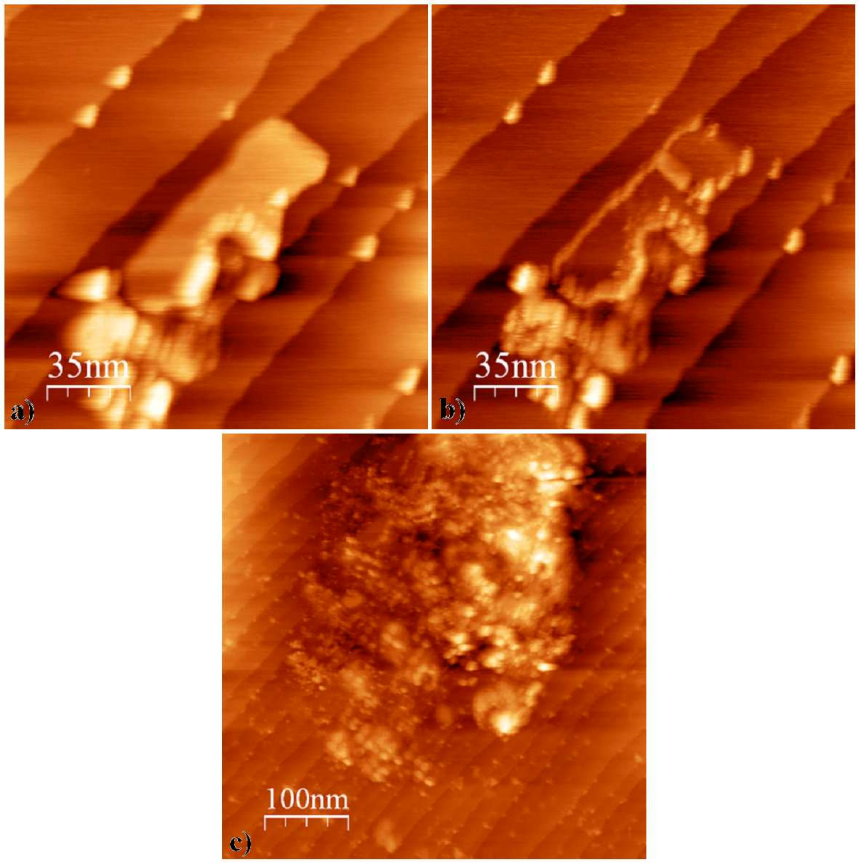

Fig. 3. STM images of 0.6 ML Sm/Mo(110) at positive and negative biases. 180×180 nm^2, $U = 2$ V, $I_t = 0.22$ nA (a); 180×180 nm^2, $U = -2$ V, $I_t = 0.25$ nA (b); 500×500 nm^2, $U = 2$ V, $I_t = 0.22$ nA (c).

For Sm coverages higher than 1 ML, the effect of different imaging vs. bias polarity is less pronounced, but is still discernible. Figure 4 shows STM images obtained for $\theta = 1.7$ ML with positive (a) and negative (b) bias voltages. Profiles recorded within the same area for both images (Fig. 4c) reveal certain differences in apparent heights of the terraces. In particular, the height of the terrace, measured between bright-and-bright or dark-and-dark parts, is of 2.2 ± 0.1 Å, and does not

depend on the bias polarity. This value is equal to that obtained for the height of terraces of a clean Mo(110) surface, and therefore it seems reasonable to suggest that the Sm layers just overbuild the Mo terraces. However, the height of Sm islands (measured between dark and bright areas) occurs significantly different when estimated with positive and negative biases. Namely, with a positive bias the estimated height of the island is 3.3 ± 0.1 Å while with a negative bias it increases to 4.1 ± 0.1 Å.

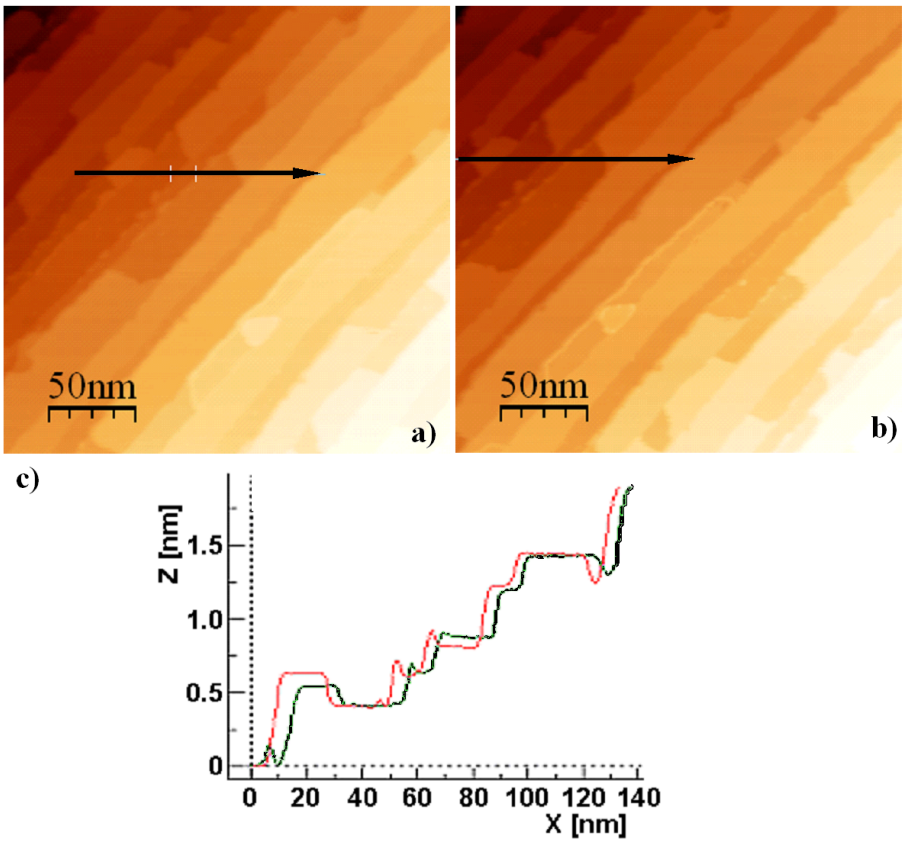

Fig. 4. STM images of 1.7 ML Sm/Mo(110) at positive and negative biases. 350×250 nm^2, $U = 2$ V, $I_t = 1$ nA (a); 250×250 nm^2, $U = -2$ V, $I_t = 1$ nA (b); profile along lines in part (a) — light and (b) — dark (c).

The STM images obtained with positive and negative biases for low Sm coverages on Mo(211) are quite similar. Only after exceeding the 0.6 ML Sm coverage the layers are imaged differently for positive and negative bias voltages. The STM images obtained for $\theta = 0.7$ ML are shown in Fig. 5.

For a positive bias, the surface is imaged as smooth terraces with several holes in each (Fig. 5a). However, a negative bias reveals a well developed surface

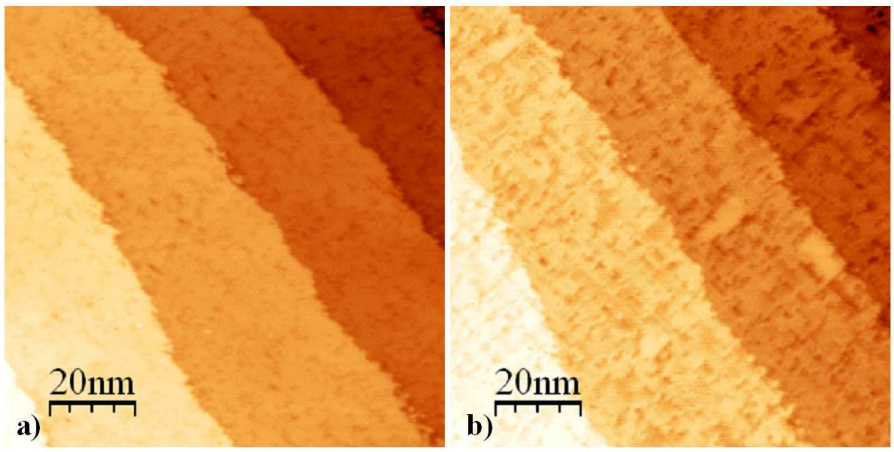

Fig. 5. STM images of 0.7 ML Sm/Mo(211) at positive and negative biases. 100×100 nm^2, $U = 2$ V, $I_t = 0.5$ nA (a); 100×100 nm^2, $U = -2$ V, $I_t = 0.5$ nA (b).

relief (Fig. 5b). The height of the terraces is found to be of 1.2 ± 0.1 Å (again, this can be understood as Sm overbuilds the Mo(211) terraces), independently of bias polarity. For a negative bias, some rectangular islands, 0.6 ± 0.1 Å height, are visible, while they become invisible for opposite bias. The borders of these islands are parallel to the $[1\bar{1}0]$ and $[\bar{1}11]$ directions on the Mo(211) surface. The terraces seen in the STM images have a well developed c(2×2) structure, in which Sm atoms occupy every second adsorption site in the row. The rectangular islands have the c$(1/\theta \times 2)$ structure, in which Sm atoms along the rows are more closely packed than in the c(2×2) structure. With increasing coverage, the number of the islands increases, and they cover the entire surface.

It should be noted that defects, seen in the STM pictures obtained for Sm coverage $d = 1$ ML, for a negative bias are imaged as holes (0.5 ± 0.1 Å depth) in smooth areas (Fig. 6a), while for a positive bias they get transformed to small islands (Fig. 6b). STM images for thick ($\theta > 1$ ML) layers do not depend on the polarity of bias. A detailed mechanism of the growth of Sm layers on the Mo(211) surface is discussed elsewhere [38, 39].

The dependence of the Sm/Mo(211) surface imaging on polarity of the bias appears for the coverage range that corresponds to the minimum of work function [38, 39]. The work function minimum relates to the beginning of the metallization of adsorbed layers, which reveals itself in the appearance of characteristic plasmon losses in LEED spectra [40]. It should be noted that the Sm layer on Mo(112) is non-uniform, that is, consists of rather dense (probably, metallic) islands forming over otherwise more dilute c(2×2) structure of the layer. Because of different electronic structures, the domains will be imaged differently and this can explain the dependence of the STM images on the polarity of bias.

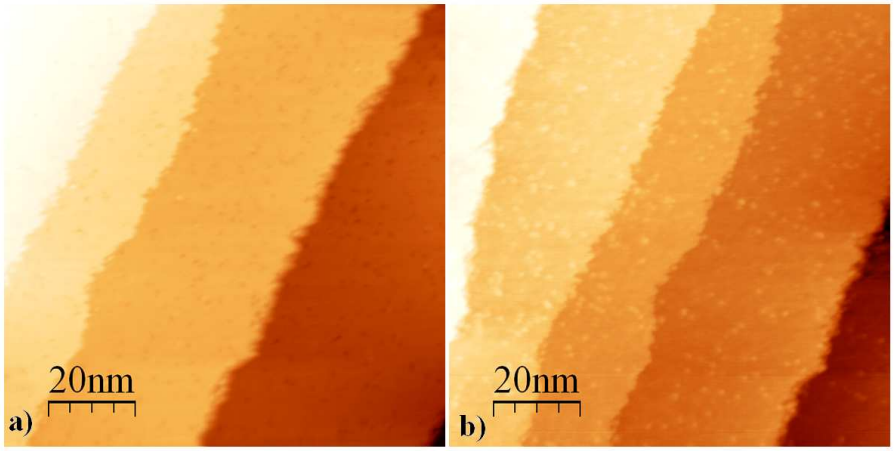

Fig. 6. STM images of 1 ML Sm/Mo(211) at negative and positive biases. 100×100 nm^2, $U = -2$ V, $I_t = 1$ nA (a); 100×100 nm^2, $U = 2$ V, $I_t = 1$ nA (b).

A similar dependence of STM images on polarity of the bias was observed for Sm layers adsorbed on semiconductors [27–29]. This effect was attributed to semiconducting properties of the substrate. Hence, it seems possible that hydrogen contamination could be responsible for the different imaging of Sm layers also on Mo surfaces. It has been found [41] that hydrogen desorption from highly hydrated Sm occurs at 870 K, while the operating temperature of the samarium source is about 700 K, so that some hydrogen contamination of deposited Sm cannot be excluded. In this case, forming Sm hydrides might result in semiconducting electronic structure of deposited layer, thus explaining the appearance of the dependence of STM images on bias polarity. For this reason we have studied the composition of surface layers by means of thermodesorption spectroscopy (Fig. 7).

Figure 7 presents TDS spectra of thick Sm layers on Mo(110) surface (part (a)), together with H signal (part (b)). Samarium has 5 stable isotopes: ^{144}Sm (3.07%), ^{149}Sm (13.82%), ^{150}Sm (7.38%), ^{152}Sm (26.75%) and ^{154}Sm (22.75%) [42]. We choose the masses between 152 and 156 to check Sm and SmH_x fluxes, because the isotopes 152 and 154 are the most intensive. The range of investigated masses includes Sm^+ (152 and 154 a.m.u.), SmH^+ (153 and 155 a.m.u.), SmH_2^+ (154 and 156 a.m.u.), and SmH_3^+ (155 a.m.u.), so if there were some SmH_x there should be signals at 153, 155 and 156 a.m.u., accordingly to the hydride state. Recorded TDS spectra are identical with TDS spectra published in [18]. The signal from the mass 153 represents the same behavior as for masses 152 and 154 and originates from the overlap of very strong signals from ^{152}Sm and ^{154}Sm. If the signal from mass 153 came from SmH, the same run should be for the mass 155, but the mass 155 remains at the background level during the net thermodesorption process. The same is valid for SmH_2 where masses 154 and 156 originate from SmH_2 created by ^{152}Sm and ^{154}Sm isotopes. SmH_3 in this range of masses is

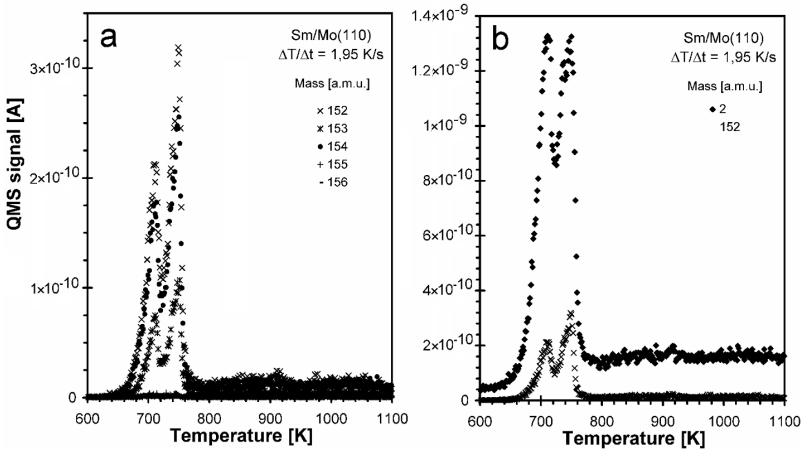

Fig. 7. TDS spectra of thick Sm layer on Mo(110) surface (a) and the hydrogen signal (b).

represented only by the mass 155 (for ^{152}Sm) and, as mentioned above, the signal from the mass 155 remains on the background level.

Figure 7b presents the signal from the molecular hydrogen together with the ^{152}Sm signal. Both curves look similar, both peaks are in the same position in the temperature scale. There are several possible explanations of such behavior. It cannot be excluded that hydrogen comes from the adsorbed Sm layer or segregates from the bulk of Mo. The sample holder or QMS also could be a source of hydrogen. Also, a possible formation of negative SmH_x ions, which are undetectable by the standard QMS, cannot be excluded. Another possibility is that in QMS, the SmH_x complexes undergo dissociation instead of ionization. In this case the mass spectrometer will show Sm and H signals, which cannot be distinguished from the desorption of separate Sm and H atoms.

4. Summary

It has been found that obtained images of Sm layers adsorbed on Mo(110) and (211) surfaces significantly depend on the polarity of the STM bias voltage. This dependence is more pronounced for Sm/Mo(110) than for Sm/Mo(211). In particular, at low Sm coverages on Mo(110), when LEED indicates forming c(7×2) structure, the change of bias polarity results in significant difference in the measured height of the adsorbed Sm layer while the heights of substrate terraces remain the same for both signs of the applied bias voltage. In the coverage range $0.65 < \theta < 1$, STM images, obtained with negative bias, show the gaps in Sm layers, which are invisible for positive bias. For Sm on Mo(211), in the coverage range $0.65 < \theta < 1$ ML, the STM images, obtained with a negative bias, show deep gaps in the Sm layer, which are not visible for positive bias.

The performed TDS study of Sm layers has not provided a clear evidence for formation of Sm hydrides on the Mo(110) surface, which could be responsible for different imaging of Sm layers with inverse bias voltages. Certainly more experiments are needed, including the study of Sm adsorption in a controlled hydrogen atmosphere, using also the STS for analysis of surface electronic structure.

Acknowledgments

The authors want to thank Prof. J. Kołaczkiewicz for his kind help in the measurements and interpretation of experimental data. This work was supported by University of Wrocław under grant No. 2016/W/IFD/08.

References

[1] G. Binnig, H. Rohre, C. Gerber, E. Weibel, *Phys. Rev. Lett.* **50**, 120 (1983).

[2] G. Binnig, H. Rohre, *Rev. Mod. Phys.* **59**, 615 (1987).

[3] G. Binnig, H. Rohre, *IBM J. Res. Dev.* **30**, 279 (1986).

[4] G. Binnig, H. Rohre, *Rev. Mod. Phys.* **71**, S324 (1999).

[5] J. Tersoff, D.R. Hamann, *Phys. Rev. B* **31**, 805 (1985).

[6] K.E. Johnson, R.J. Wilson, S. Chiang, *Phys. Rev. Lett.* **71**, 1055 (1993).

[7] R. Koller, W. Bergermayer, G. Kresse, C. Kovicka, M. Schmid, J. Redinger, R. Podloucky, P. Varga, *Surf. Sci.* **512**, 16 (2002).

[8] R.-P. Blum, H. Niehus, C. Hucho, R. Fortrie, V. Ganduglia-Pirovano, J. Sauer, S. Shaikhutdinov, H.-J. Freund, *Phys. Rev. Lett.* **99**, 226103 (2007).

[9] N.V. Petrova, I.N. Yakovkin, *Phys. Rev. B* **76**, 205401 (2007).

[10] S.D. Barrett, S.S. Dhesi, *The Structure of Rare-Earth Metal Surfaces*, Imperial College Press, London 2001.

[11] Ya.B. Losovyj, I.N. Yakovkin, S.D. Barrett, T. Komesu, P.A. Dowben, *Surf. Sci.* **520**, 43 (2002).

[12] R. Pascal, Ch. Zarnitz, M. Bode, R. Wiesendanger, *Phys. Rev. B* **56**, 3636 (1997).

[13] R. Pascal, Ch. Zarnitz, M. Bode, R. Wiesendanger, *Surf. Sci.* **385**, L990 (1997).

[14] R. Pascal, Ch. Zarnitz, M. Bode, M. Getzlaff, R. Wiesendanger, *Appl. Phys. A* **65**, 603 (1997).

[15] R. Pascal, C. Zarnitz, H. Tödter, M. Bode, M. Getzlaff, R. Wiesendanger, *Appl. Phys. A* **66**, S1121 (1998).

[16] I.N. Yakovkin, *Surf. Sci.* **601**, 1001 (2007).

[17] A. Rosengren, B. Johansson, *Phys. Rev. B* **26**, 3068 (1982).

[18] A. Stenborg, E. Bauer, *Surf. Sci.* **185**, 394 (1987).

[19] A. Stenborg, O. Bjorneholm, A. Nilsson, N. Martensson, J.N. Andersen, C. Wigren, *Phys. Rev. B* **40**, 5916 (1989).

[20] E. Lundgren, J.N. Andersen, R. Nyholm, X. Torrelles, J. Rius, A. Delin, A. Grechnev, O. Eriksson, C. Konvicka, M. Shmid, P. Varga, *Phys. Rev. Lett.* **88**, 136102 (2002).

[21] C.L. Nicklin, M.J. Evarard, C. Norris, S.L. Bennett, *Phys. Rev. B* **70**, 235413 (2004).

[22] L. Tao, E. Goering, S. Horn, M.L. denBoer, numaPhys. Rev. B481528993.

[23] D.M. Jaffey, A.J. Gellman, R.M. Lambert, *Surf. Sci.* **214**, 407 (1989).

[24] Y. Nakayama, H. Kondoh, T. Ohta, *Surf. Sci.* **552**, 53 (2004).

[25] Y. Nakayama, H. Kondoh, T. Ohta, *Surf. Sci.* **600**, 2403 (2006).

[26] C. Wigren, J.N. Andersen, R. Nyholm, M. Gothelid, M. Hammar, C. Tornevik, U.O. Karlsson, *Phys. Rev. B* **48**, 11014 (1993).

[27] F. Palmino, E. Ehert, L. Mansour, E. Duverger, J.-C. Labrune, *Surf. Sci.* **586**, 56 (2005).

[28] C. Ohbuchi, J. Nogami, *Surf. Sci.* **579**, 157 (2005).

[29] S. Chang, P. Philip, A. Wall, A. Raisnen, N. Troullier, A. Franciosi, *Phys. Rev. B* **35**, 3013 (1987).

[30] P. Vajda, *Handbook on the Physics and Chemistry of Rare Earths*, Vol. 20, Eds. K.A. Gschneidner Jr., L. Eyring, Elsevier Science, Amsterdam 1995, p. 207 and references therein.

[31] J. Opyrchal, Ph.D. Thesis, INTiBS PAN, 1979.

[32] E. Nowicka, R. Nowakowski, R. Duś, *Appl. Surf. Sci.* **254**, 4346 (2008).

[33] M. Di Vece, A.M.J. van der Eerden, J.A. van Bokhoven, S. Lemaux, J.J. Kelly, D.C. Koningsberger, *Phys. Rev. B* **67**, 035430 (2003).

[34] R. Griessen, *Europhys. News* **32**, 42 (2001).

[35] R. Pascal, Ch. Zarnitz, M. Bode, R. Wiesendanger, *Phys. Rev. B* **59**, 8195 (1999).

[36] I.N. Yakovkin, M. Kuchowicz, R. Szukiewicz, J. Kołaczkiewicz, *Surf. Sci.* **600**, L240 (2006).

[37] I. Horcas, R. Fernandez, J. M. Gomez-Rodríguez, J. Colchero, J. Gómez-Herrero, A.M. Baro, *Rev. Sci. Instrum.* **78**, 13705 (2007).

[38] M. Kuchowicz, Ph. D. Thesis, U.Wr., 2007.

[39] M. Kuchowicz, J. Kołaczkiewicz, in preparation.

[40] J. Kołaczkiewicz, E. Bauer, *Surf. Sci.* **265**, 39 (1992).

[41] N. Yoshihiro, J. Kadono, S. Nishiuchi, S. Yamamoto, T. Tanabe, H. Miyake, *J. Alloys Comp.* **408-412**, 355 (2006).

[42] http://www.webelements.com/webelements/elements/text/Sm/isot.html.